Hierarchical Modeling of the Dynamics of Polymers with a Nonlinear Molecular Architecture: Calculation of Branch Point Friction and Chain Reptation Time of H-Shaped Polyethylene Melts from Long Molecular Dynamics Simulations

Nikos Ch. Karayiannis and Vlasis G. Mavrantzas*

Department of Chemical Engineering, University of Patras, Patras GR 26504, Greece & Institute of Chemical Engineering and High-Temperature Chemical Processes, FORTH-ICE/HT, Patras GR 26504, Greece

Received May 12, 2005; Revised Manuscript Received July 17, 2005

ABSTRACT: Thoroughly equilibrated atomistic configurations of H-shaped polyethylene (PE) melts, obtained through a novel implementation of the double-bridging Monte Carlo algorithm [Karayiannis et al. *J. Chem. Phys.* **2003**, *118*, 2451], have been subjected to equilibrium *NPT* molecular dynamics (MD) simulations at $T = 450$ K and $P = 1$ atm, for times up to 4 μs. The simulated model H-shaped systems consist of PE chains possessing a main backbone (a "crossbar") trapped between two branch points each of which is linked to two dangling arms. In our simulations, the average number of carbon atoms in the backbone ranged from 48 up to 300 corresponding to both unentangled and entangled crossbars, while the average arm length was kept relatively small (it ranged from 24 up to 50) corresponding always to unentangled arms. Our long MD simulation studies reveal the different relaxation mechanisms exhibited by an H-polymer: the rapid relaxation due to arm breathing (on the order of a few nanoseconds for the short, unentangled arms considered here, up to C_{50}) and the slow branch point diffusion (on the order of a few microseconds for the size of the entangled backbones considered here, up to C_{300}), which, in turn, governs the sluggish diffusive motion of the entire H-molecule. Analysis of the curves describing the time decay of the autocorrelation functions for the unit vectors directed from the branch point to the free end of the arm and from one branch point to the other reveals a number of relaxation modes, indicative of the strong cooperativity between arm and backbone relaxations in H-shaped structures. It is further observed that once Fickian diffusion is established, the mean-square displacement (msd) of the chain center-of-mass follows remarkably faithfully that of branch points. This validates from first principles the assumption of the pom-pom model [Bishko et al. *Phys. Rev. Lett.* **1997**, *79*, 2352] that all friction in an H-polymer is concentrated at the two branch points. Values of the branch point friction coefficient, ζ_b, a significant parameter entering the pom-pom model, have also been calculated. For the longest H-polymers studied, logarithmic plots of the msd of the inner crossbar segments against time are seen to exhibit the four different regimes predicted by the reptation theory of Doi−Edwards for entangled linear polymer melts, with corresponding exponents remarkably close to those of the theory. This allowed us to extract the characteristic relaxation times τ_e, τ_R, and τ_d of the theory for all simulated systems and the value of the effective diameter, a, of the underlying tube model.

1. Introduction

Polymer melts with long-chain branching exhibit rheological properties that differ substantially from those of linear melts, particularly in extensional flows where long-chain branching leads to extreme strain hardening. In contrast, the shear rheology of long-chain branched (LCB) liquids is very shear thinning, much like that of unbranched, linear polymers or of polymers with side branches too short to entangle with surrounding chains.[1−6]

In the literature, the special rheology (strain hardening in extension, strain softening in shear) of such polymers has been attributed to material that lies between branch points. According to McLeish and collaborators,[2,3,7] it is the presence of multiple branch points on the same molecule, which gives rise to molecular strands with no free ends, that is mainly responsible for the strain hardening exhibited by LCB molecules. Building on this and the tube model for entangled polymer melts,[8,9] Bishko et al.[1] and McLeish and Larson[2] formulated a novel molecular theory for the rheology of an (idealized) class of LCB polymers termed "pom-pom" molecules. These are generalizations of the H-polymer structure[6,10−12] made up by a single backbone ("crossbar") from the two ends of which a number q of branches emerge. H-structures constitute the simplest pom-pom model with $q = 2$.

According to the pom-pom model, stress relaxation in an H-polymer proceeds through a 3-stage mechanism: (a) At early times, stress relaxes by path length fluctuation in the dangling arms, controlled by the rapid Rouse motion of free ends along the tube. (b) At longer times, the rapid path length fluctuations cross over to an exponentially slow "activated diffusion" regime for the deeper arm fluctuations. (c) After the starlike arms have completely retracted, relaxation proceeds via renormalized reptation of the crossbars in a dilated tube defined by their mutual entanglements.

The pom-pom model is a remarkably successful theory of the dynamics and rheology of H-shaped melts[13] and of the more complex comblike polymers.[14] It leads to a tractable integro-differential constitutive equation that predicts rheological properties in shear and extensional flow astonishingly similar to those of, for example,

* Corresponding author. E-mail: vlasis@chemeng.upatras.gr. Telephone: +30-2610-997-398. Fax: +30-2610-965-223.

10.1021/ma050989f CCC: $30.25
Published on Web 08/30/2005

Table 1. Details of the Simulated H-Shaped PE Melt Systems (T = 450 K, P = 1 atm)

system	no. of chains	no. of interacting sites	arm MW (g/mol)	backbone MW (g/mol)	total MW (g/mol)	polydispersity index (backbone/arms)
H_48_24	40	5760	337	670	2018	1.083/1.083
H_78_24	32	5568	337	1090	2438	1.083/1.083
H_78_48	16	4320	673	1090	3782	1.083/1.083
H_128_24	24	5376	337	1790	3138	1.083/1.083
H_128_48	16	5120	673	1790	4482	1.083/1.083
H_300_50	16	8000	701	4198	7002	1.053/1.053

typical low-density polyethylene melts.[2] Key to its success have been the assumptions that all fast relaxation is confined to the arms, and that at long times all of the effective friction to curvilinear (reptation) motion of the pom-pom backbones is located at the branch points (rather than distributed along the chain). None of the two assumptions has, however, been tested from first principles; they have been proposed and accepted on the basis of the idealized pom-pom model and the remarkable success of the tube model of entanglements. In this paper, we present qualitative proof for the validity of the two assumptions based on direct observation of the chain long time dynamics through extensive, equilibrium molecular dynamics (MD) simulations with model H-shaped polyethylene (PE) melt systems, preequilibrated at all length scales through a novel Monte Carlo (MC) algorithm.[15−17]

In the literature, the simulation of nonlinear polymer melt architectures has been restricted to the study of small alkane systems bearing short branches along their main backbone.[18−25] H-shaped PE polymers have been simulated by Zhang et al.[26] who studied their crystallization behavior and how it compares against that of linear ones, and by Jabbarzadeh et al.[27] who reported on the effect of molecular shape on the Couette shear flow of comb, star, and H-shaped PE melts. For the more complex dendrimers, Zacharopoulos and Economou[28] have performed equilibrium atomistic MD simulations in order to investigate characteristics of molecular structure and morphology in the melt, while Bosko et al.[29,30] have studied the viscoelastic properties of dendrimers of generation 1−4 using nonequilibrium MD.

Simulations of long, entangled polymeric systems with a nonlinear molecular architecture became possible only very recently thanks to a novel design and implementation of the class of chain-connectivity altering MC algorithms known as "double bridging" (DB) and "intramolecular double rebridging" (IDR)[15,16] that allowed equilibrating model H-shaped PE melts at all length scales.[17] DB and IDR are in fact applicable not only to LCB but also to many other macromolecular systems such as cyclic peptides, terminally grafted polymers, chain systems with stiff backbones, mixtures of star and linear polymers,[31] and/or infinite-length chain molecules, provided their chemistry remains simple; the simulation of all of these architectures is almost impossible with conventional MC or MD methods.[32] In particular, by properly redesigning the two moves to allow for bridgings between (a) the main backbones of two different chains, (b) the arms of two different chains, and (c) the branches of the same chain, and by introducing special moves (such as the H−BR[17] and the double ConRot[17]) to effect atom displacements at the junction points, a novel MC algorithm arises capable of simulating long H-shaped PE melts (molecular weight (MW) up to 9500 g/mol) in atomistic detail.[17] In addition to predicting the thermodynamic, volumetric and conformational properties of H-polymers,[17] the new MC algorithm has provided a large number of totally uncorrelated and fully equilibrated (at all length scales) configurations of H-shaped PE melts for subsequent dynamic studies. Results from these (dynamic) studies are presented in the following sections of this paper.

2. Molecular Model and Systems Studied

The H-shaped melt systems simulated in this work are denoted as H_*x*_*y* where *x* and *y* represent the average number of carbon atoms per backbone and arm, respectively, and are all characterized by a uniform distribution of molecular lengths (separately for the backbone and their four dangling arms). The following systems have been simulated: a 40-chain H_48_24, a 32-chain H_78_24, a 24-chain H_78_48, a 24-chain H_128_24, a 16-chain H_128_48, and a 16-chain H_300_50 PE melt. A detailed description of their molecular characteristics (total number of chains and interacting sites in the simulation box, backbone and arm molecular weights, and polydispersity indices) is given in Table 1. To compare against the dynamics of linear analogue PE melts (melts of the same arm, backbone or total molecular length), a number of linear systems, ranging in molecular length from C_{24} up to C_{500}, have also been simulated.

All MD simulations have been conducted in the *NPT* equilibrium ensemble at $T = 450$ K and $P = 1$ atm using the LAMMPS (large-scale atomic/molecular massively parallel simulator) software (version LAMMPS 2001 in Fortran 90).[33,34] For the integration of the equations of motion, the multiple time step algorithm rRESPA[35,36] was employed with the small integration time step set equal to 1 fs and the large one equal to 5 fs. In all simulations, the Nosé−Hoover thermostat and the Andersen barostat were employed. The total MD duration was 1 μs for the shorter and 4 μs for the longer (e.g., the H_300_50) systems.

The molecular model employed in the simulations is very similar to that used in our previous studies of linear and nonlinear PE melts,[15−17] providing excellent estimates of their volumetric and conformational properties for a variety of temperature conditions. It adopts the united-atom representation according to which all CH, CH_2, and CH_3 units are treated as single, spherically symmetric interacting sites. In the model, all intramolecular interactions between sites separated by more than three bonds along a chain as well as all intermolecular ones are described by a 12−6 Lennard-Jones (LJ) potential whose ϵ and σ values for the CH_2 and CH units are borrowed from the TraPPE[37] and Nath−Khare[38] models, respectively. As far as the ϵ and σ values for the CH_3 units are concerned, these have been taken to be identical to those for the CH_2 ones. Standard Lorentz−Berthelot combining rules have been used to describe nonbonded interactions between sites of different kind. Bond lengths have been taken to

Table 2. Atomistic Molecular Model and Values of the Parameters of Its Potential Functions Describing All Inter- and Intramolecular Interactions

type of interaction and potential function	type of interacting site	parameter values
bond lengths	CH_x-CH_2	$l_0 = 1.54$ Å
$V_{stretch}(l)/k_B = 1/2\ k_l(l - l_0)^2$	($x = 1, 2, 3$)	$k_l = 96500$ K Å^{-2}
nonbonded interactions	CH_x	$\epsilon_{CH_x}/k_B = 46\ K$, $\sigma_{CH_x} = 3.95$ Å
$V_{LJ}(r_{ij}) = 4\epsilon_{ij}[(\sigma_{ij}/r_{ij})^{12} - (\sigma_{ij}/r_{ij})^6]$	($x = 2, 3$)	
	CH	$\epsilon_{CH}/k_B = 39.7$ K, $\sigma_{CH} = 3.85$ Å
bond bending	$CH_x-CH_2-CH_2$	$k_\theta = 62500$ K rad^{-2}, $\theta_0 = 114°$
$V_{bend}(\theta)/k_B = {}^1/_2 k_\theta(\theta - \theta_0)^2$	(x = 1, 2, 3)	
	$CH_2-CH-CH_2$	$k_\theta = 62500$ K rad^{-2}, $\theta_0 = 109.47°$
dihedral angles	CH_x-$CH_2-CH_2-CH_2$	$N = 8$, $c_0 = 1001$ K,
$V_{tor}(\phi)/k_B = \sum_{i=0}^{N} c_i \cos^i(\phi)$	($x = 1, 2, 3$)	$c_1 = 2130$ K, $c_2 = -303$ K, $c_3 = -3612$ K, $c_4 = 2227$ K, $c_5 = 1966$ K, $c_6 = -4489$ K, $c_7 = -1736$ K, $c_8 = 2817$ K
$V_{tor}(\phi)/k_B = c_0 + \sum_{i=1}^{3} c_i(1 + d_i \cos(i\varphi))$	$CH_2-CH-CH_2-CH_2$	$c_0 = 1416.3$ K, $c_1 = 398.3$ K, $c_2 = 139.12$ K, $c_3 = -901.2$ K, $d_1 = +1$, $d_2 = -1$, $d_3 = +1$

fluctuate harmonically around a mean value of 1.54 Å according to the Nath et al. model,[38,39] while bond angles have been assumed to obey the Van der Ploeg and Berendsen bending potential.[40] As far as the torsional potential is concerned, dihedrals of the kind $CH_x-CH_2-CH_2-CH_2$ ($x = 1$, 2 or 3) have been assumed to be governed by Toxvaerd's nine-term, sum-of-cosines formula,[41] while dihedrals around the $CH-CH_2$ bonds have been sampled according to the potential function proposed by Nath and Khare.[38] The mathematical expressions and the corresponding parameters for all kinds of potential interactions encountered in the present simulations are summarized in Table 2.

3. Results

3.1. Computational Efficiency. The superiority of the MC algorithm[17] based on the DB and IDR[15,16] moves to the state-of-the-art MD method (fully parallelized with the rRESPA time step integrator[35,36] as incorporated in the LAMMPS code[33,34]) in equilibrating the long-range characteristics of the simulated H-shaped PE melts is documented in Figure 1. The figure presents the decay of the orientational autocorrelation function (ACF) for the unit vector directed from one branch point to the other, $\langle \mathbf{r}_b(t)\cdot\mathbf{r}_b(0)\rangle/\langle r_b{}^2\rangle$, as a function of CPU time, for the simulated H_128_24, H_128_48, and H_300_50 systems. Reported CPU times correspond to single runs on an 8-node Linux cluster of dual Intel Xeon workstations at 2.8 GHz with a 1GB memory. Also shown in the figure is the ACF curve corresponding to the longest H_300_50 melt as obtained from the present MD simulations executed in parallel on all 8 nodes of the cluster. The rate with which the ACF curve drops to zero is a measure of how fast the backbone of the H-shaped molecule "forgets" its initial configuration, i.e., of its equilibration rate. The MC method, based on the DB and IDR chain-connectivity-altering moves,[15,16] is seen to be by 2 orders of magnitude more efficient than the parallel MD method in equilibrating the long-length scale characteristics of the H_300_50 system. What is also important about the curves in Figure 1 is that the performance of the MC algorithm (in equilibrating the orientational features of the main backbone) is independent of the arm molecular length; furthermore, it increases as the molecular length of the backbone increases. This is an outstanding feature of the new algorithm, reminiscent of that exhibited by the end-bridging (EB)[42,43] or DB and IDR algorithms[15,16] in simulations of linear polydisperse or monodisperse systems,[44] allowing for the study of the volumetric and conformational properties of a number of long H-shaped PE melts.[17]

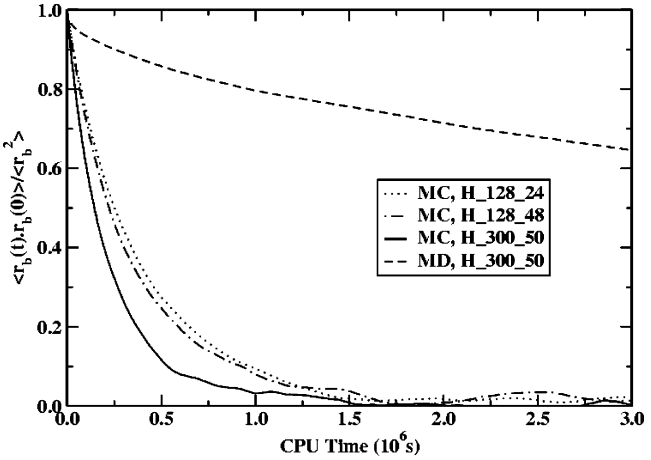

Figure 1. Decay of the autocorrelation function for the unit vector directed from one branch point to the other, $\langle \mathbf{r}_b(t)\cdot\mathbf{r}_b(0)\rangle/\langle r_b{}^2\rangle$, with CPU time (on a single Intel Xeon processor at 2.8 GHz) for the simulated H-shaped PE melts, with the new chain-connectivity altering MC algorithm. Also shown is the curve obtained for the H_300_50 system with the *NPT* MD algorithm executed in parallel on a cluster of 8 Intel Xeon nodes at 2.8 GHz. [$T = 450$ K, $P = 1$ atm].

Equilibrated configurations obtained at the end of the MC simulations were subsequently subjected to long MD simulations in the *NPT* statistical ensemble to study their equilibrium dynamic properties. All initial configurations were carefully chosen so as to be characterized by a uniform distribution of backbone and arm lengths, with dimensions (as quantified through the chain radius of gyration) and density equal to those obtained from the MC simulations. Detailed results from these MD simulation studies are presented in the next sections.

3.2. Orientational Relaxation of Backbones and Arms. Time Autocorrelation Functions. Figure 2a presents the time decay of the orientational autocorrelation function (ACF) in linear coordinates for the unit vector directed from one branch point to the free end of the corresponding dangling arm, $\langle \mathbf{r}_a(t)\cdot\mathbf{r}_a(0)\rangle/\langle r_a{}^2\rangle$, as obtained from the present *NPT* MD simulations for all simulated H-shaped PE melts. The $\langle \mathbf{r}_a(t)\cdot\mathbf{r}_a(0)\rangle/\langle r_a{}^2\rangle$ time autocorrelation function expresses the rate with which

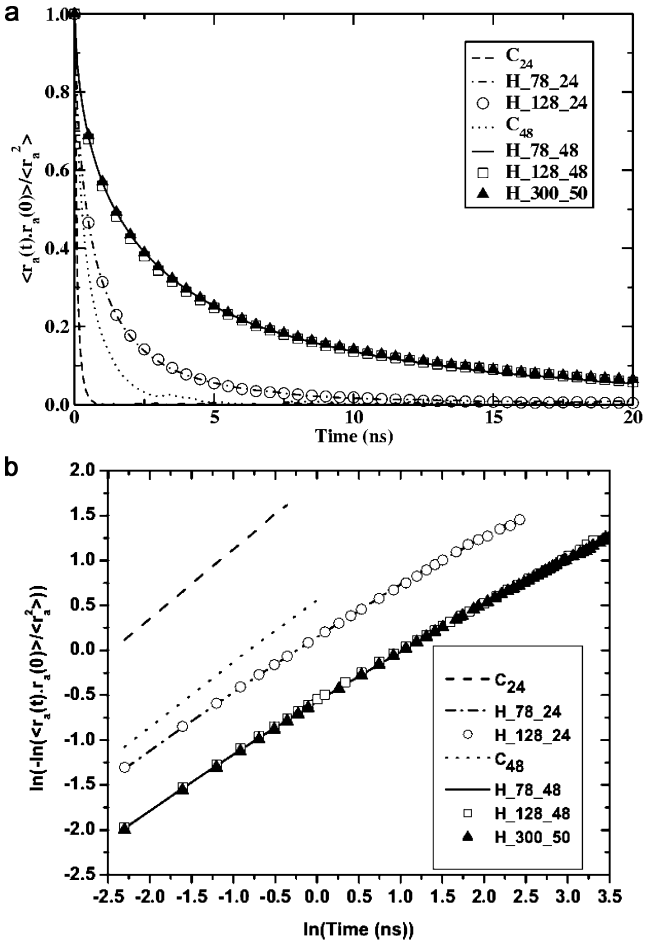

Figure 2. (a) Decay of the time autocorrelation function (ACF) for the unit vector directed from one branch point to the free end of the adjacent dangling arm(s), $\langle \mathbf{r}_a(t)\cdot\mathbf{r}_a(0)\rangle/\langle r_a{}^2\rangle$, for the simulated H-shaped PE melts as obtained by the present *NPT* MD simulations (T = 450 K and P = 1 atm), in linear coordinates. Also shown are the corresponding curves for the end-to-end unit vector of linear PE melts of length equal to that of the arms (C_{24} and C_{48}, respectively). (b) Same as part a but in a ln(−ln(ACF))-vs-ln(t) scale.

the corresponding arms lose the memory of their initial conformation. Also reported in Figure 2a are the corresponding time ACF's obtained from *NPT* MD simulations with linear PE systems of chain length C_{24} and C_{48}, i.e., equal to the arm length, N_a, of the simulated H-polymers. Dangling arms are always seen to relax slower than their "free" linear-chain analogues of the same molecular length, by almost 1 order of magnitude. It is also observed that the curves depicting the time ACF's for arms exhibit a rapid decay at short times followed by a rather slow relaxation at longer times. To subsequently investigate if only a single or more than one processes characterize arm relaxation, Figure 2b presents again plots of the time decay of the $\langle \mathbf{r}_a(t)\cdot\mathbf{r}_a(0)\rangle/\langle r_a{}^2\rangle$ ACF but this time in a ln(−ln(ACF))-vs-ln(t) scale. Interestingly enough, in these coordinates one sees two relaxation processes: a short-time process describing arm reorientational characteristics for times up to a characteristic time t_0 ($\approx$ 1 ns for both the C_{24}- and C_{48}-long arms studied here), and a wider arm relaxation process for times beyond t_0.

To make quantitative the dependence and variation of the two relaxation processes on the molecular features of the studied systems, the $\langle \mathbf{r}_a(t)\cdot\mathbf{r}_a(0)\rangle/\langle r_a{}^2\rangle$ curves have been fitted piecewise with stretched exponential (KWW) functions of the form

$$\frac{\langle \mathbf{r}_a(t)\cdot\mathbf{r}_a(0)\rangle}{\langle r_a{}^2\rangle} = \exp\left[-\left(\frac{t}{t_{\mathrm{KWW}}}\right)^{\beta}\right] \tag{1}$$

which (as Figure 2b shows) follow the simulation data quite accurately. t_{KWW} and β in (1) are the two fitting parameters of the KWW function. Once t_{KWW} and β have been obtained, one can readily calculate also the value of the (total) correlation time, t_c, as the integral of the time ACF from $t = 0$ up to $t \rightarrow \infty$:

$$t_c = \int_0^{\infty} \frac{\langle \mathbf{r}_a(t)\cdot\mathbf{r}_a(0)\rangle}{\langle r_a{}^2\rangle} \mathrm{d}t \tag{2}$$

Values of the fitting parameters (t_{KWW}, β) for the two processes and the corresponding total correlation time, t_c, for arm relaxation in all simulated systems are reported in Table 3. For comparison, in Table 4, we report the corresponding t_{KWW}, β, and t_c values characterizing the single time decay of the orientational autocorrelation function of the chain end-to-end unit vector in systems of linear PE melts having the same molecular length, C_{24} and C_{48}, with the arms studied here.

For times $t < t_0$, the dangling arms of the H-molecule exhibit a rather rapid relaxation (characterized by β values between 0.66 and 0.63 for the C_{24} and C_{48} arm lengths studied here), which is independent of backbone length. For times $t > t_0$, the mode of arm relaxation crosses over to a wider process characterized by lower β values that now depend on backbone length. This reveals the cooperativity between arm and backbone relaxation processes (see also the discussion below) in H-polymers. At short time ($t < t_0 \approx 1$ ns), arms relax as having one of their ends (the branch point) firmly fixed (i.e., totally immobile), which explains why the characteristic KWW β values in the earlier stages of relaxation are always smaller than those of the corresponding free linear analogues. At these short times, most of the relaxation is due to the outer end of the arm which is completely free to dangle around and sample the available configuration space. For times $t > t_0$, further arm relaxation can occur only if the branch point diffuses away, that is through a cooperative mechanism with the backbone (which by nature is attached to it). It is this need for a cooperativity with backbone relaxation, mediated by their sluggishly diffusing common branch point, that causes the change in arm relaxation mode at time t around t_0, and drives arm relaxation at later times (beyond t_0). It is also observed that the total arm (de)correlation time, t_c, is practically independent of the molecular length and mass fraction of backbone material, being mainly a strong function of arm molecular length, N_a. This is due to the short chain length of the simulated arms, which in all cases studied here is below the critical length N_e ($\approx$ 170) for the formation of entanglements. In contrast, in highly entangled H-shaped polymers, McLeish and Larson propose that the arm relaxation time should be a strong function not only of arm molecular length, N_a, but also of arm (or, equivalently, backbone) material fraction, φ_a. Simulations with H-structures bearing entangled arms are currently in progress to investigate these dependencies further. Total correlation times for arm relaxation are

Table 3. Values of the Characteristic Relaxation Time, t_{KWW}, and Stretching Exponent, β, of the KWW (Kohlrausch−Williams−Watts) Functions Employed to Analytically Fit in a Piecewise Fashion the Decay of the Time Autocorrelation Function (ACF) of the Unit Vector Directed from One Branch Point to the Free End of the Dangling Arm, Describing *Arm* Orientational Relaxation in the Simulated H-Shaped PE Melts (T = 450 K and P = 1 atm)

	1st arm relaxation process		2nd arm relaxation process		
system	t_{KWW} (ns)	β	t_{KWW} (ns)	β	t_c (ns)
H_48_24	0.60	0.66	0.63	0.58	1.3
H_78_24	0.73	0.66	0.72	0.55	1.3
H_128_24	0.74	0.65	0.74	0.55	1.3
H_78_48	2.3	0.63	2.7	0.54	5.5
H_128_48	2.2	0.63	2.7	0.52	5.5
H_300_50	2.3	0.63	2.7	0.51	5.5

Table 4. Same as with Table 3 but for the Time ACF of the Chain End-to-end Unit Vector Describing Orientational Relaxation in Melts of *Linear* PE Systems of Molecular Length Similar to that of the H-Polymers Simulated Here (T = 450 K, P = 1 atm)

	1st relaxation process		2nd relaxation process		3rd relaxation process		
system	t_{KWW} (ns)	β	t_{KWW} (ns)	β	t_{KWW} (ns)	β	t_c (ns)
C_{24}	0.09	0.74					0.13
C_{48}	0.44	0.72					0.58
C_{78}	1.4	0.66					1.8
C_{122}	4.0	0.60					6.1
C_{142}	5.1	0.59					7.0
C_{174}	7.0	0.61	10	0.54	9.7	0.69	13
C_{224}	11	0.61	17	0.54	26	0.65	27
C_{270}	15	0.61	35	0.48	27	0.62	33
C_{320}	22	0.61	66	0.45	66	0.63	81
C_{500}	38	0.61	190	0.39	157	0.62	420

Table 5. Same as with Table 3 but for the Time ACF of the Unit Vector Directed from One Branch Point to the Other, Describing *Backbone* Orientational Relaxation

	1st backbone relaxation process		2nd backbone relaxation process		3rd backbone relaxation process		
system	t_{KWW} (ns)	β	t_{KWW} (ns)	β	t_{KWW} (ns)	β	t_c (ns)
H_48_24	9.6	0.60	7.4	0.77			8.7
H_78_24	19	0.59	13.6	0.81			16
H_128_24	60	0.57	34.5	0.79			39
H_78_48	25	0.58	53.6	0.49	35	0.80	39
H_128_48	46	0.57	124	0.48	62	0.69	64
H_300_50	310	0.57	2910	0.42	600	0.62	580

further observed to be considerably longer than those for their linear analogues. For example (see Table 4), the correlation times for the "free" C_{24} and C_{48} PE melts are equal to 0.13 and 0.58 ns, respectively, as compared to 1.3 and 5.5 ns (reported in Table 3) for C_{24}- and C_{48}-long PE segments, respectively, linked as dangling arms to the branch points of an H-shaped chain.

Figure 3 extends the study of orientational relaxation in the simulated H-polymers to the calculation of the time ACF for the unit vector directed from one branch point to the other (i.e., along the main backbone), $\langle \mathbf{r}_b(t)\cdot\mathbf{r}_b(0)\rangle/\langle r_b^2\rangle$, for the shorter (H_48_24, H_78_24, and H_78_48) and longer (H_128_24, H_128_48, and H_300_50) simulated systems, respectively. Part a of Figure depicts the time decay of the ACF in linear coordinates and part b in a "ln(−ln(ACF))-vs-ln(t)" scale. Similarly to arm relaxation, backbone relaxation is characterized by more than one processes: two in the case of the smaller (H_48_24, H_78_24, and H_128_24), and three in the case of the longer (H_78_48, H_128_48, and H_300_50) simulated H-systems. The different relaxation modes are well described by KWW functions of the form of eq 1, with values of the corresponding characteristic times t_{KWW} and stretching exponents β as reported in Table 5; also reported in Table 5 are the total backbone correlation times, t_c, for all simulated systems. For comparison, in Table 4 we have included the corresponding t_{KWW}, β, and t_c values characterizing the different relaxation processes and total correlation time for the chain end-to-end unit vector in systems of linear PE melts of molecular length equal to backbone (N_b) or total (N_b + $4N_a$) chain length of the simulated H-structures.

Early orientational relaxation in backbones is characterized by β exponents with values between 0.57 and 0.60 rather independently of the molecular characteristics (N_a, N_b, φ_a, and MW) of the H-molecule. These values are systematically smaller than the β values characterizing early time orientational relaxation in free linear analogues, indicative of the restricted motion of backbones (the "crossbars") as they are firmly attached to the highly immobile branch points. The intermediate regime, observable only in the longer systems (H_78_48, H_128_48, and H_300_50), is a wider relaxation process, which now exhibits a strong dependence on the molecular length of the backbone, N_b: the higher the value of N_b the wider the relaxation process. This resembles the behavior of the respective entangled linear systems (see Table 4), and suggests an influence on backbone relaxation of entanglements with other backbones or H-chains, thus further hindering its motion (in excess to that due to the two sluggishly diffusing branch points). On the other hand, the terminal relaxation backbone mode is a rather narrow process, as now the diffusion of the branch points has freed a significant portion of constraints. KWW β values here are very similar to those characterizing terminal orientational relaxation in linear melts of the same (high) MW

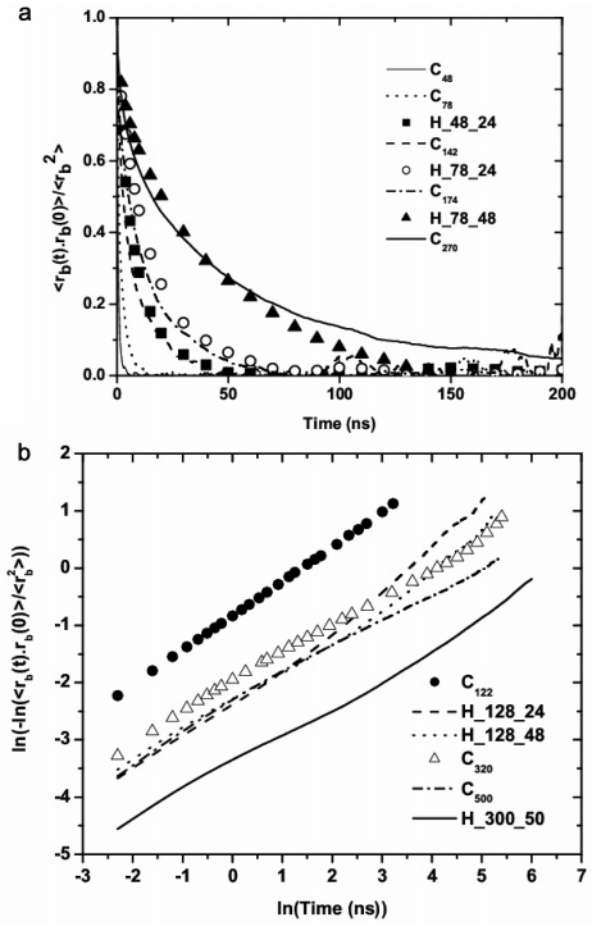

Figure 3. (a) Decay of the time autocorrelation function for the unit vector directed from one branch point to the other, $\langle \mathbf{r}_b(t)\cdot\mathbf{r}_b(0)\rangle/\langle r_b^2\rangle$, for the smaller H-shaped PE melts (H_48_24, H_78_24, and H_78_48) as obtained from the present *NPT* MD simulations ($T = 450$ K and $P = 1$ atm), in linear coordinates. Also shown are the corresponding curves for the end-to-end unit vector of linear PE melts with length equal to that of either the total H-molecule (C_{142}, C_{174} and C_{270}) or its main backbone (C_{48} and C_{78}). (b) Same as part a but for the longer H_128_24, H_128_48, and H_300_50 PE systems in a ln(−ln(ACF))-vs-ln(t) form.

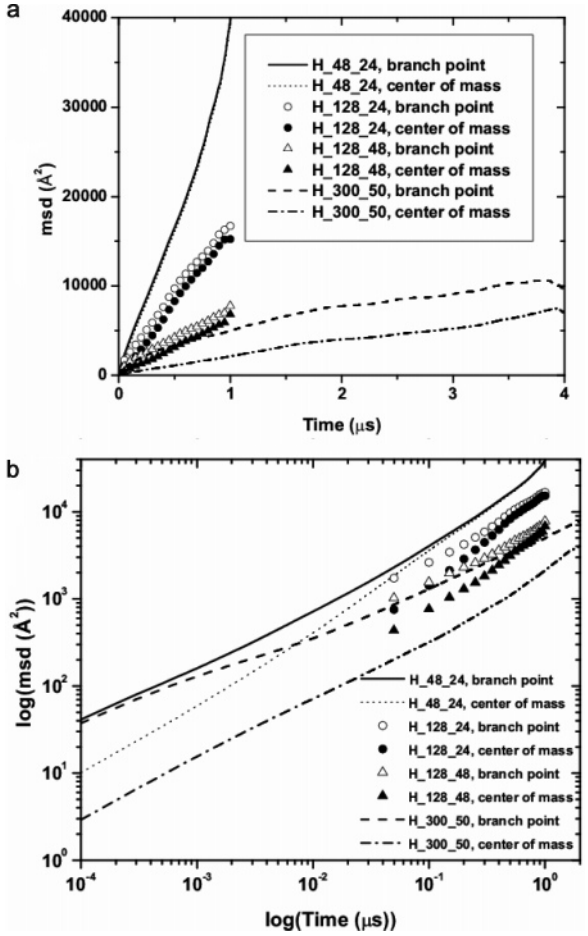

Figure 4. Mean-square displacement (msd) of the chain center-of-mass and of each one of the two branch points as a function of time for the simulated H-shaped PE melts, in linear (a) and logarithmic (b) coordinates ($T = 450$ K, $P = 1$ atm).

(compare, for example, the similarities in the terminal relaxation of the H_300_50 and the linear C_{500} PE systems), which underlines the dominant role of long-lived topological constraints (entanglements) in the system dynamics.

The curves of Figure 3 and the data of Table 4 reveal that (again, in contrast to the short-arm orientational relaxation analyzed above) the rate with which backbones relax is a strong function of their own molecular length, N_b, but also of the arm molecular length, N_a. This rate is, as in the case of the arms, systematically slower by 1 order of magnitude than that observed in "free" linear-chain analogues (C_{48}, C_{78}, C_{128}, and C_{300}). This is in excellent qualitative agreement with the McLeish−Larson theory[2] for highly entangled H-shaped molecules, which proposes a linear dependence of backbone relaxation time on the longest arm relaxation time (or, equivalently, an exponential dependence on N_a). It is concluded that the presence of the four arms (even if they are too short to be entangled) has a profound effect on the dynamics of H-polymers, dramatically slowing down the relaxation rate of their backbones. For example, as N_b increases from 128 (in the H_128_48 system) to 300 carbon atoms (in the H_300_50 system), Table 5 shows t_c to increase from 64 to 580 ns, indicative of the behavior of a backbone crossing most probably over to the entanglement regime. At present, simulations with longer H-shaped melts bearing not only entangled backbones but also entangled arms are in progress to test more rigorously the proposed pom-pom analytical formulas for the dependence of backbone and arm relaxation times on the molecular parameters of the H-molecule.

3.3. Chain Self-Diffusivity. Branch Point Friction. The diffusive behavior of the H-shaped chains is examined in Figure 4 showing the mean square displacement (msd) of the chain center of mass, $\langle[\mathbf{R}_G(t) - \mathbf{R}_G(0)]^2\rangle$, and of branch points, $\langle[\mathbf{R}_b(t) - \mathbf{R}_b(0)]^2\rangle$, in time for the H_48_24, H_128_24, H_128_48, and H_300_50 PE systems, in linear (part a) and logarithmic (part b) coordinates. The long time scales up to which the simulations have been carried out (exceeding 4 μs in some of them) has ensured that branch points (except for those of the very long H_300_50 system whose dynamics is dramatically slow) and chains centers-of-mass have diffused for distances at least 3 times longer that their average dimension and that Fickian diffusion has well set-in (to reliably compute diffusion coefficients) in all cases. The curves shown in Figure 4 demonstrate chains centers-of-mass msd's following astonishingly closely those of branch points: For the shorter H-polymer studied (H_48_24), the two msd curves travel in time exactly one next to other right from the very

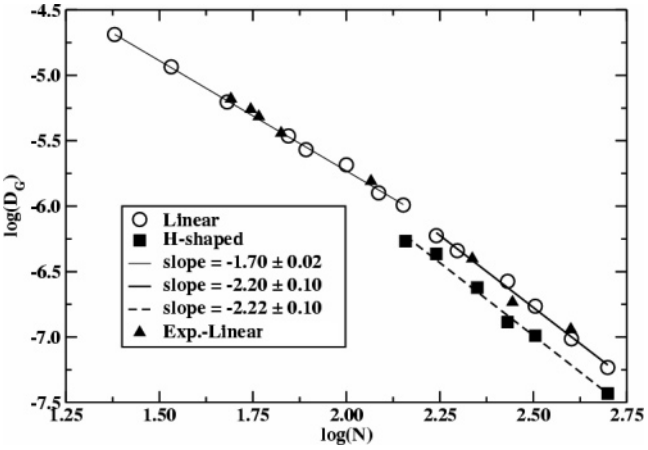

Figure 5. Chain center-of-mass self-diffusion coefficient, D_G, (in cm^2/s) vs chain length N in a log−log plot for the H-shaped PE melts as obtained from the present *NPT* MD simulations (T = 450 K, P = 1 atm). Also shown are data from MD simulations and experimental measurements for a number of linear PE systems under the same conditions (T = 450 K, P = 1 atm).

beginning. For the longer systems (H_128_24, H_128_48, and H_300_50), this happens after the initial period of the usual sub-diffusive behavior (which is more pronounced in the msd curves of the branch points) has elapsed. Such a result validates the main assumption of the McLeish−Larson theory that, at long times, indeed, *the effective friction to curvilinear motion is all located at the branch points* (rather than distributed along the molecule's main backbone and branches).

Significant information about the long-time dynamics of the simulated H-shaped PE systems is further provided by the dependence of the chain self-diffusion coefficient, D_G, on chain molecular length (or, equivalently, MW). In the hydrodynamic limit when Fickian diffusion is established, D_G is calculated through the Einstein relation

$$D_G = \lim_{t\to\infty} \frac{\langle [\mathbf{R}_G(t) - \mathbf{R}_G(0)]^2 \rangle}{6t} \qquad (3)$$

The values of D_G obtained and their dependence on average molecular length, N, for all simulated H-shaped PE melts are shown in a log−log plot in Figure 5. The figure reports results also for the chain self-diffusion coefficient of a number of linear polydisperse PE systems, of average chain length up to N = 500 carbon atoms, under the same conditions (T = 450 K, P = 1 atm), as obtained either from parallel *NPT* MD simulations on linear systems (I = 1.053) or as measured experimentally.[45] Similarly to past[46] and more recent[47] simulation studies with other linear PE and *cis*-1,4-polybutadiene (PB) systems, a gradual, very smooth change in the slope of the power-law dependence of D_G on chain length N is recorded at an intermediate value of N (between C_{140} and C_{170} in Figure 5) marking the passage from a Rouse- to a reptation-like behavior: For chain lengths N below C_{140}, chain end effects combine with Rouse dynamics[48] to result in D_G values that exhibit a power-law dependence on N of the form $D_G \propto N^{-b}$ with b = 1.70 (±0.05). For chain lengths N above C_{170}, reptation dynamics dominates chain mobility, resulting in D_G values that exhibit a stronger dependence on N, described again by a power-law of the form $D_G \propto N^{-b}$ but now with b = 2.20 (±0.10). The value of 2.20 for b is in excellent agreement with the recent experimental data reported by Tao et al.,[49] Pearson et al.,[45,50] Lodge[51] and Wang[52] for PE and many other polymers.

Table 6. Values of Branch Point Diffusivity, D_b, and Branch Point Friction Constant, ζ_b, for the H-Shaped PE Melt Systems Studied Here (T = 450 K, P = 1 atm)[a]

system	D_b (10^{-7} cm^2/s)	ζ_b (10^{-12} N s/cm)
H_48_24	5.5	1.1
H_78_24	4.7	1.3
H_78_48	1.5	4.1
H_128_24	3.1	2.0
H_128_48	1.4	4.4
H_300_50	0.49	13

[a] D_b has been calculated from the slope of the branch point msd-vs-t curve in the terminal (or Fickian diffusion) regime (eq 3 in the main text), whereas ζ_b has been extracted from the corresponding pom-pom equation (eq 4 in the main text)

A remarkable feature in the curves of Figure 5 is that the same exponent, b = 2.22 (±0.10), describes the power-law dependence of D_G on N, also for the nonlinear H_*x*_*y* PE melts simulated in the present work, despite their different values of backbone and arm lengths (totally different values of arm material fraction, φ_a). This is a significant result, since it suggests that an H-polymer can behave as entangled irrespective of the individual values of its backbone and arm lengths, especially if it possesses a linear segment of length $N_a + N_b + N_a$ whose molecular length is larger than N_e. For example, the H_128_48 PE melt behaves as entangled despite the fact that, separately, the molecular lengths of its main backbone (C_{128}) and of each one of its four arms (C_{48}) are below N_e. On the basis of the data of Figure 5 for the power-law dependence of D_G on N, all H-shaped PE melts simulated here behave as entangled except possibly for the H_48_24 (whose total chain length, C_{144}, is below N_e).

According to McLeish and Larson the value of the branch point diffusion coefficient, D_b, can be used to extract an estimate for the branch point friction coefficient, ζ_b, through an Einstein argument:[2]

$$\zeta_b = \frac{k_B T}{D_b} \qquad (4)$$

Results for D_b and ζ_b for all simulated H-shaped PE melts (at T = 450 K, P = 1 atm) are reported in Table 6. The ζ_b values, in particular, show a strong dependence on N_b and N_a; furthermore, they are all on the order of 10^{-12} N s cm^{-1} and higher, i.e., considerably larger than the value calculated for the total chain friction coefficient in past MD simulations with linear PE melts at the same temperature.[46] This demonstrates the large friction concentrated at the branch points of an H-shaped PE molecule as compared to the friction felt by a monomer along a linear PE chain as it diffuses through the sea of the rest of the monomers.

3.4. Segmental Motion. The Brownian motion of polymers can be experimentally studied by dynamic light scattering. By measuring the time correlation of the scattered light, one can extract the dynamic structure factor, which provides important information about correlations in the msd of polymer segments in the system. Structural relaxation in a polymer melt is also investigated with other techniques such as quasi elastic neutron scattering (QNS) and neutron spin echo (NSE). Data from NSE experiments about the dynamic struc-

ture factor are directly comparable to our MD simulation data for the single chain incoherent dynamic structure factor, since they are also connected with correlations in segmental displacements. Particular attention is paid here on the characteristic features of the msd of individual polymer segments, $\phi_n(t)$: according to the reptation theory of polymer dynamics for entangled systems, a log−log plot of $\phi_n(t)$ against t exhibits the following four distinct regions:

•A very short time behavior where the segment does not feel the constraints of the network and $\phi_n(t)$ scales with time t as $t^{1/2}$ (Rouse motion in free space). This behavior is correct for times t shorter than the characteristic time τ_e ($t \leq \tau_e$) when the segmental displacement becomes comparable to the tube diameter a; τ_e denotes the onset of the effect of topological constrains on segmental motion.

•For times t such that $\tau_e < t < \tau_R$ where τ_R is the Rouse time of the diffusing segment, the motion of the segment perpendicular to the primitive path is restricted but that along the path remains free. The resulting diffusive behavior in this case is a consequence of the Rouse-like motion of the segment combined with the tube constraints, and $\phi_n(t) \sim t^{1/4}$.

•For times t such that $\tau_R < t < \tau_d$, where τ_d is the (disentanglement or disengagement or) reptation time, the dynamics is identical to that predicted by the primitive chain dynamics and $\phi_n(t) \sim t^{1/2}$.

•For $t > \tau_d$, the dynamics is governed by the reptation process and $\phi_n(t) \sim t$.

The above scalings are summarized as follows:[9]

$$\phi_n(t) \propto \begin{cases} t^{1/2} & t \leq \tau_e \\ t^{1/4} & \tau_e \leq t \leq \tau_R \\ t^{1/2} & \tau_R \leq t \leq \tau_d \\ t^{1} & \tau_d \leq t \end{cases} \quad (5)$$

We have calculated segmental msd's for all the simulated H-shaped PE melts, and the results obtained with the shorter (H_48_24, H_78_24, and H_128_24), the intermediate (H_78_48 and H_128_48) and the longer (H_300_50) simulated PE systems are shown on a log−log plot against time in parts a−c of Figure 6. To get rid of effects associated with the dynamics of the two branch points, all plots have been obtained by averaging only over the innermost backbone segments, lying up to 19 bonds away from the center of the backbone. [Exploratory $\phi_n(t)$ calculations with the H_300_50 PE melt based on the msd of an expanded ensemble of carbon atoms lying up to 39 bonds around the central backbone atom in each backbone yielded identical curves.]

For the smaller H-shaped systems studied (H_48_24, H_78_24, and H_128_24), three distinct regimes are observed in Figure 6a characterized by slopes equal to 0.55 ± 0.02, 0.40 ± 0.03, and 1, respectively. As the MW of the H-molecule increases (H_78_48 and H_128_48 systems in Figure 6b), the intermediate Rouse regime is seen to gradually split up into two sub-regimes; for these systems the values of the characteristic exponents are 0.55 ± 0.02, 0.35 ± 0.03, 0.50 ± 0.01, and 1, respectively. For even longer H-molecules (e.g., the H_300_50 PE melt analyzed in Figure 6c), the $\phi_n(t)$-vs-t curve is seen to exhibit three characteristic breaks marking transitions between different time behaviors,

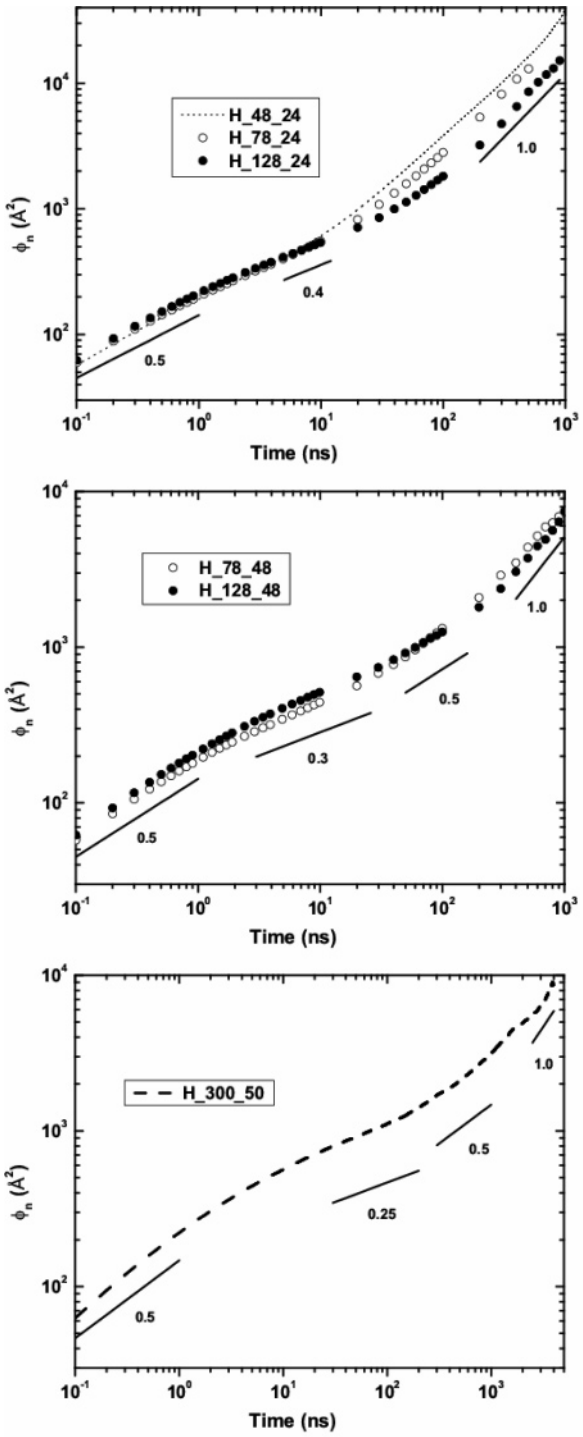

Figure 6. (a) Mean square displacement of the innermost backbone segments, ϕ_n, as a function of time in a logarithmic plot for the simulated H_48_24, H_78_24, and H_128_24 systems ($T = 450$ K, $P = 1$ atm). The three solid lines with slopes equal to 0.5, 0.4, and 1.0, respectively, have been drawn to serve as guides for the eye. (b) Same as with Figure 6a but for the H_78_48 and H_128_48 systems. The four solid lines with slopes equal to 0.5, 0.3, 0.5, and 1.0 have again been drawn to serve as guides for the eye. (c) Same as with Figure 6a but for the longer H_300_50 system. Here, too, the four solid lines with slopes equal to 0.5, 0.25, 0.5, and 1.0 have been drawn to serve as guides for the eye.

characterized by exponents that are practically the same with those suggested by the reptation theory.[9] In general, it is predicted that as long as the total chain length of the simulated H-shaped PE melts is longer

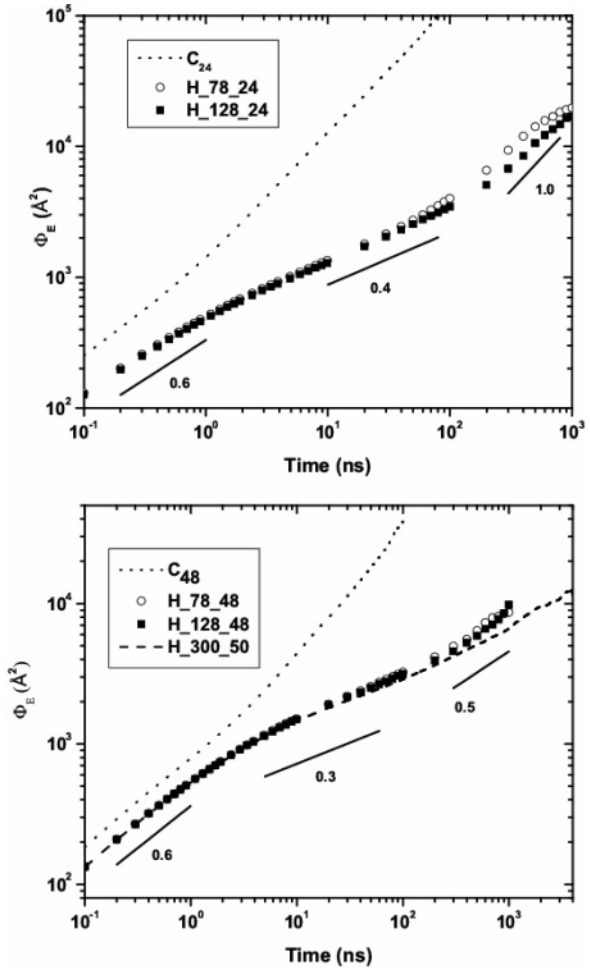

Figure 7. (a) Mean square displacement of the free ends of the four dangling arms, ϕ_e, as a function of time in logarithmic scale for the H_78_24 and H_128_24 systems. Also shown is the corresponding curve for a linear C_{24} system having the same number of carbon atoms as each of the four arms of the simulated H-polymers. [$T = 450$ K, $P = 1$ atm]. (b) Same with part a but for the H-systems bearing arms with average molecular length $N_a = 48$ (H_78_48, H_128_48, and H_300_50).

than C_{224} (the total chain length of the H_128_24 system), all four breaks are present in the logarithmic plots of the segmental displacements against time. For the H_300_50 PE system, the scaling laws predicted by our *NPT* MD simulations can be summarized as follows:

$$\phi_n(t) \propto \begin{cases} t^{0.55\pm0.02} & t \le \tau_e \\ t^{0.27\pm0.02} & \tau_e \le t \le \tau_R \\ t^{0.50\pm0.02} & \tau_R \le t \le \tau_d \\ t^{1} & \tau_d \le t \end{cases} \quad (6)$$

On the basis of the information provided by the $\phi_n(t)$-vs-t curves, and in full consistency with the results for the chain length dependence of the chain self-diffusion coefficient (see Figure 5), it is concluded that, except possibly for the shorter H_48_24 PE melt, the rest of the simulated systems (H_128_24, H_128_48, and H_300_50) behave as entangled.

In Figure 6a−c we have discussed the msd of the innermost backbone segments of the simulated H-shaped melts. Of interest is also the time behavior of the msd of the free ends of the four dangling arms, $\phi_e(t)$; these are shown in parts a and b of Figure 7. Also

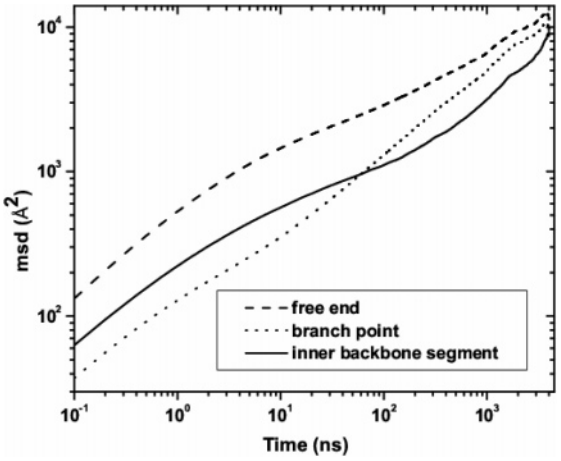

Figure 8. Mean square displacement of free ends, branch points and innermost backbone segments as a function of time for the H_300_50 system in a log−log scale ($T = 450$ K, $P = 1$ atm).

shown in the same figure are the corresponding ϕ_e-vs-t curves for linear analogues having the same molecular length as the arms of the simulated H-melts. The dynamics of the free ends in the two cases is totally different. When the two ends are the free ends of linear C_{24} and C_{48} chains, $\phi_e(t)$ exhibits two distinct time-behaviors: a short-time ($t < 1$ ns) where $\phi_e(t) \sim t^n$ with $n = 0.74$ for the C_{24} and $n = 0.61$ for the C_{48} melt, and a long-time behavior (corresponding to the Fickian diffusion limit) where $n = 1$ for both of them. On the other hand, when the two ends are the free ends of the arms of an H-shaped molecule, the function $\phi_e(t)$ exhibits more breaks indicative of a more complex system dynamics: there is a short-time ($t < 1$ ns) behavior where $\phi_e(t) \sim t^n$ with $n = 0.6$ for both the C_{24} and C_{48} arms in all simulated systems, then there exists one intermediate regime for the C_{24}-long arms where $n = 0.4$, and at least two for the C_{48}-long arms with n equal to 0.30 and 0.50, respectively, and of course there exists the long time limit of Fickian behavior where $n = 1$; the latter was reached in our simulations only in the case of the shorter-arm (C_{24}) H-molecules. In contrast, in the C_{48}-long arm systems, the Fickian limit was never observed, even after 4 μs. Given this, the possibility for the existence of additional intermediate regimes in the $\phi_e(t)$-vs-t curves of these systems should not be excluded.

The different time patterns exhibited by the msd's of all different groups of atoms encountered in an H-shaped polymer (free ends, branch points and inner backbone segments) are collectively shown and compared against each other in Figure 8. The data have been obtained from our 4 μs-long MD simulation with the H_300_50 PE system and are indicative of the rich dynamics characterizing segmental motion and diffusion in melts of entangled H-shaped polymers.

3.5. Characteristic Segmental Relaxation Times. Tube Diameter. That segmental motion in entangled H-polymers agrees with the specific diffusive behavior predicted by the reptation theory[9] for entangled linear polymer melts is a significant result of the present work. Among others, the log−log plots of the $\phi_n(t)$-vs-t curves of Figure 6 can be used to calculate the three characteristic times τ_e, τ_R (Rouse time), τ_d (reptation time) and the corresponding effective diameter a of the tube model. The values computed for the longer (H_128_48 and H_300_50) systems are reported in Table 7. Also

Table 7. Values of the Three Characteristic Times (τ_e, τ_R, and τ_d) of the Reptation Theory, and of the Corresponding Mean-Square Segmental Displacements ($\phi_n(\tau_e)$, $\phi_n(\tau_R)$ and $\phi_n(\tau_d)$) for Inner Backbone Atoms of H-Shaped PE Melts As Obtained from the Current *NPT* MD Simulations (T = 450 K, P = 1 atm)[a]

system	$\langle R_b^2 \rangle$ (Å^2)	τ_e (ns)	ϕ_n (τ_e) (Å^2)	τ_R (ns)	$\phi_n(\tau_R)$ (Å^2)	τ_d (ns)	ϕ_n (τ_d) (Å^2)	a (Å)
H_128_48	2300	1.5 ± 0.3	270	46 ± 10	860	295 ± 50	2800	29 ± 2
H_300_50	5900	2.8 ± 1.0	350	228 ± 40	1490	2230 ± 300	5300	32 ± 2

[a] Also listed are the values of the mean square distance from one branch point to the other, $\langle R_b^2 \rangle$, for each system, and the effective diameter of the tube model, a, extracted by mapping our MD simulation data onto the tube model (see eq 7 in the main text).

reported in Table 7 are the following: (a) the values $\phi_n(\tau_e)$, $\phi_n(\tau_R)$, and $\phi_n(\tau_d)$ of the msd's of inner backbone segments at times $t = \tau_e$, τ_R, and τ_d, respectively, and (b) the values of the mean square distance from one branch point to the other, $\langle R_b^2 \rangle$, the latter providing a measure of the average backbone size in each system. The effective tube diameter a can be calculated through the formula suggested by Likhtman and McLeish:[53]

$$a = \sqrt{3\phi^*} = \sqrt{3\phi_n(t^*)} \tag{7}$$

where t^* is the time where fitted straight lines through the first two scaling laws in the logarithmic plots of the segmental msd curves against time in Figure 6, parts b and c, cross each other; the corresponding msd value is denoted as ϕ^*. If t^* is known, one can also extract the value of the time τ_e denoting the onset of tube constraint effects through[53]

$$\tau_e = \frac{36}{\pi^3} t^* \tag{8}$$

As proposed by Likhtman and McLeish, eq 7 allows the calculation of the tube diameter a, either from available MD simulations[54] or neutron-spin echo (NSE) measurements of the type reported by Wischnewski et al.[55,56] The estimates obtained from our MD simulations (at T = 450 K and P = 1 atm) are (see also Table 7): $a = (2.9 \pm 0.2)$ nm for the H_128_48, and (3.2 ± 0.2) nm for the H_300_50 system. Very similar values are obtained for the corresponding linear PE analogues (melts of the same total MW).

In Table 7 it is observed (compare, e.g., the $\phi_n(\tau_d)$ and $\langle R_b^2 \rangle$ values reported therein) that in order for the innermost backbone segments along an H-molecule to escape tube constraints, they should travel for distances comparable to the dimension, $\langle R_b^2 \rangle$, of the chain backbone.

As far as the times τ_R and τ_d are concerned, the values obtained from our simulations are: $\tau_R = 46$ ns and $\tau_d = 300$ ns for the H_128_48 system, and $\tau_R = 230$ ns and $\tau_d = 2230$ ns for the H_300_50 system. These estimates are consistent with the phenomenological relationship proposed by Graessley[57] on the basis of the Doi–Edwards theory, according to which

$$\tau_d = \frac{15}{4} \frac{M}{M_e} \tau_R \tag{9}$$

with a value for the entanglement molecular weight M_e approximately equal to 2400 g/mol (estimated from the point marking the change in the slope in the logarithmic plot of the diffusion constant D_G against total chain length N in Figure 5). For the longest H_300_50 polymer, the estimated reptation time τ_d is almost 1 order of magnitude larger compared to the reptation time τ_d of a linear C_{320} PE melt with MW equal to that of its backbone. A similar conclusion is drawn if the comparison is made on the basis of the values of t_c, reported in Tables 4 and 5 for the two systems (81 and 580 ns for the C_{320} and H_300_50 systems, respectively). The observed large differences are the result of the high friction concentrated at the branch points in H-shaped polymers. As nicely explained by McLeish et al.,[3] the rapidly fluctuating arms provide drag that far outweighs the sum of monomeric drags along the backbone. Trapped between the two branch points, the main chain backbone or crossbar remains practically immobile, and it is only after very long times that arms have completely retracted that relaxation of the crossbar takes place via renormalized reptation in a dilated tube. The additional branch point friction caused by the dangling arms has a profound effect on the relaxation processes of the H-shaped molecules and its segmental dynamics even for the case of the unentangled arm systems considered here.

The values of branch point diffusivity, D_b, and tube diameter, a, reported in Tables 6 and 7, respectively, can be used to extract an estimate for the longest arm relaxation time (the time $\tau_a(0)$ for the arm free ends to retrace a path through the melt to the branch points) through the following relationship of the pom-pom model:[2]

$$\tau_a(0) = \frac{a^2}{2D_b q} \tag{10}$$

Here q denotes the number of dangling arms per backbone end ($q = 2$ for the H-shaped systems). The values obtained are: $\tau_a(0) = 150$ ns for the H_128_48 melt and 520 ns for the H_300_50 system.

3.6. Relaxational Mechanisms. The curves presented in Figures 2–4 and 6–8 are indicative of the hierarchy of relaxation mechanisms exhibited by melts of H-shaped polymer chains. If we focus our attention on the H_300_50 PE melt, in particular, the results of the present 4 μs-long MD simulations suggest the following:

(a) At very early times, only the outer arm material has relaxed by the rapid Rouse motion of the free ends; for the short arm lengths ($N_a = 50$) considered here, the time scale of this first stage of arm orientational relaxation is about 5 ns.

(b) At intermediate times, additional arm material has also relaxed by the activated path length fluctuations that cross over to an exponentially slow diffusive motion. It is at the end of this period that the diffusive motion of branch points begins. For the simulated H_300_50 system, the maximum relaxation time of the branch point was found to be close to 500 ns.

(c) At significantly longer times, following the diffusion of branch points, crossbar material (inner backbone segments) relaxes by being displaced over distances commensurate with the curvilinear length not already relaxed by fluctuation. The time scale of this terminal stage defines the reptation (or disentanglement) time

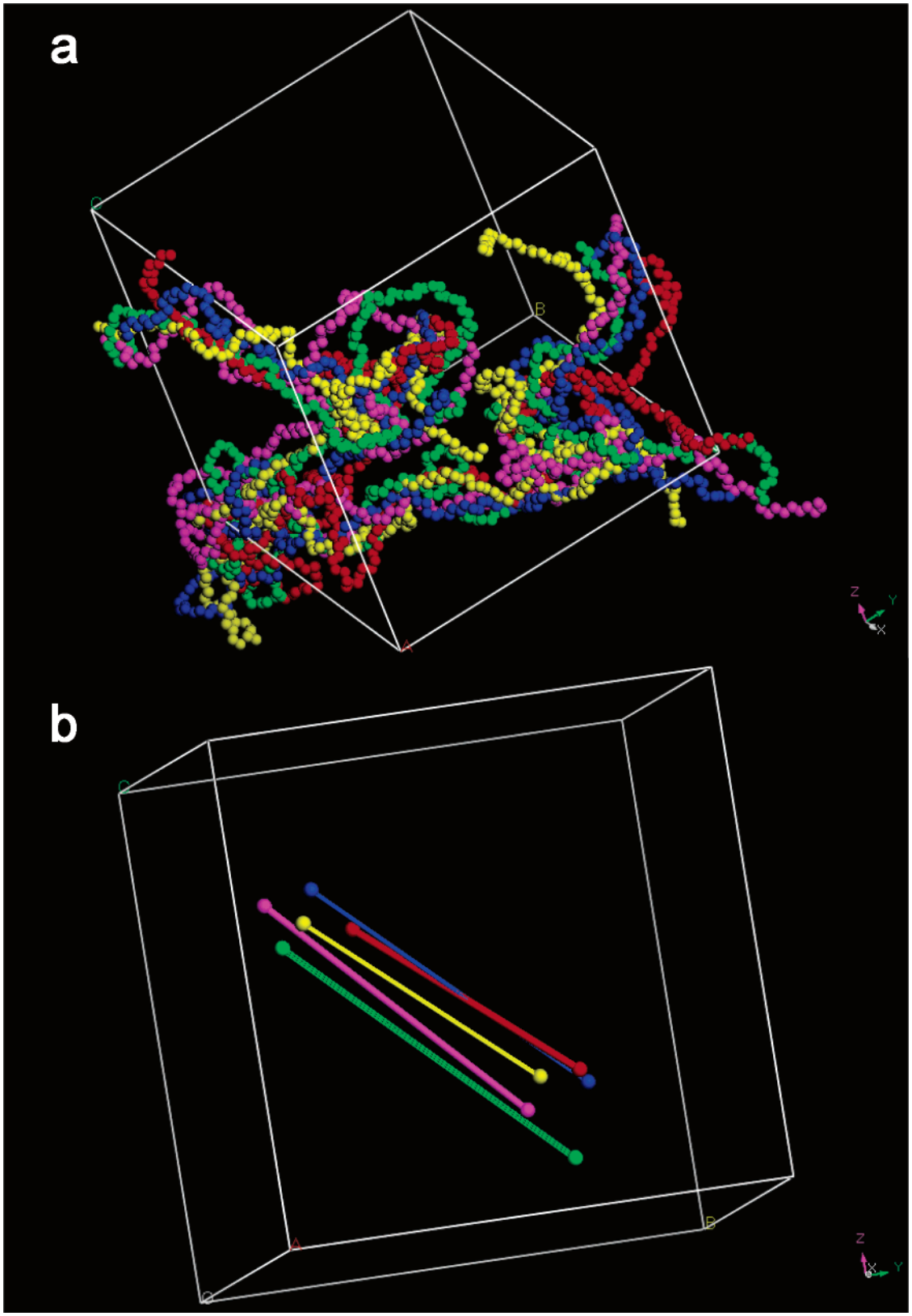

Figure 9. (a) Time series of the atomistic configuration of a randomly selected H_300_50 chain in unwrapped coordinates. Different colors are used to illustrate the different configurations that the chain assumes in time, t, as they are recorded every 0.2 ns as follows: red (at $t = 0.0$ ns), blue (at $t = 0.2$ ns), yellow (at $t = 0.4$ ns), green (at $t = 0.6$ ns), and magenta (at $t = 0.8$ ns). (b) Same as part a but now only the rod connecting the two branch points is shown, emphasizing the orientation of the backbone.

of the molecule, and for the H_300_50 melt is on the order of 2 μs.

Such a hierarchy of relaxations is schematically illustrated in Figures 9 through 11, showing the time evolution of the configuration of a randomly selected H_300_50 chain (for the purposes of visualization, the rest of the chains have been omitted), as it is recorded every 0.2 ns (Figure 9), every 10 ns (Figure 10), and

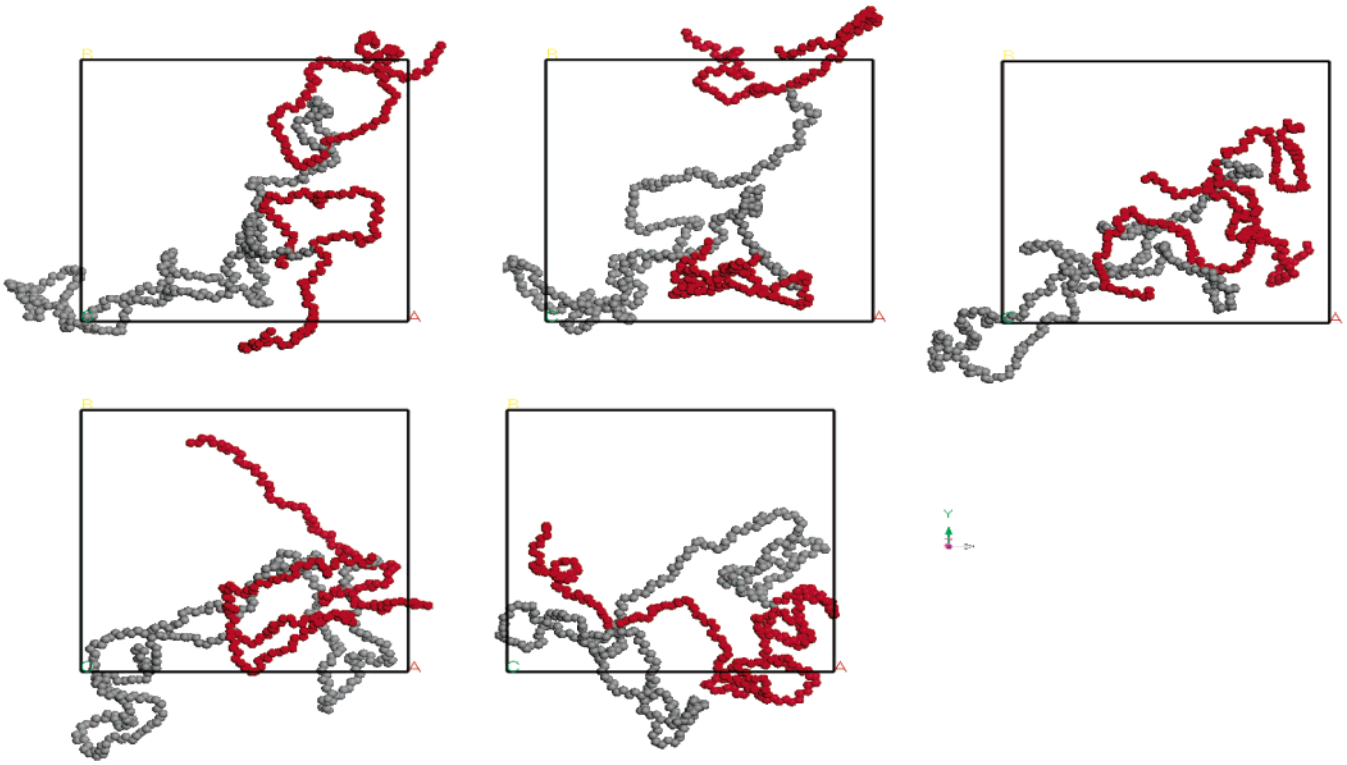

Figure 10. Time series of the atomistic configuration of a randomly selected H_300_50 chain in unwrapped coordinates. Shown in red and gray are the atoms belonging to the four arms and the backbone, respectively. The configurations are recorded in time, t, every 10 ns as follows: Top: left (at $t = 0$ ns), middle (at $t = 10$ ns), right (at $t = 20$ ns). Bottom: left (at $t = 30$ ns), middle (at $t = 40$ ns).

every 1 μs (Figure 11), from an arbitrarily selected time origin during one of our MD simulations. Part a in Figures 9 and 11 depicts the time evolution of the atomistic configuration of the chain fully unwrapped in space, while part b (of Figures 9 and 11) focuses on the evolution of the orientational characteristics of the rod connecting the two branch points. Five time snapshots are shown in each case colored in red (the 1st), blue (the 2nd), yellow (the 3rd), green (the 4th), and magenta (the 5th).

Figure 9, in particular, which spans a total time of 0.8 ns shows that within the time scale of 0.8 ns only carbon atoms near the free ends of the four arms of the molecule present significant mobility. The arm atoms near the branch points as well as all backbone material remain practically immobile: the orientation of the rod connecting the two branch points has not changed at all, which implies that branch points and all backbone atoms perform just a very short scale, local motion.

In Figure 10, on the other hand, where recordings are made every 10 ns and the total time scale spanned is 40 ns, all arm atoms have undergone significant displacements, indicative of fully relaxed arms. Within the time scale of the 40 ns, considerable mobility is also exhibited by the inner backbone segments. Interestingly enough, however, the entire H-molecule as a whole does not exhibit any diffusion: It is pinned down by the almost motionless branch points. As shown in Figure 11, extremely long times must be accessed, on the order of 4 μs, for the two branch points to diffuse away from their initial positions, and for the entire H-molecule to relax by escaping the tube constraints.

The three different time scales observed in Figures 9−11 are characteristic of the fast (related to the motion of arm free ends), intermediate (related to arm orientational relaxation) and slow (related to the motion of branch points, and, consequently, to the diffusivity of chains centers-of-mass) relaxational modes characterizing dynamics in melts of H-polymers.

4. Conclusions: Future Plans

We have presented results from 4 μs-long, atomistic *NPT* MD simulations for the equilibrium dynamic properties of model H-shaped PE melts and how they compare against those of linear melts of equivalent MW. Our simulations have allowed us to observe two different relaxation mechanisms exhibited by an H-polymer: *the fast relaxation of the free ends of the four dangling arms through a rapid Rouse-like motion* (on the order of 1 ns for the H_300_50 melt), and *the slow branch point motion accompanied by the sluggish diffusive motion of the main chain backbone through reptation* (on the order of 1μs for the H_300_50 melt). We have also demonstrated the large degree of coperativity between arm and backbone relaxation, even if the arms (and/or the backbones) are too short to be entangled. Unfortunately, due to the relatively short chain length of the arms studied here, *the intermediate relaxation of deeper segments along arms by activated path length fluctuations* was not observed.

Our MD simulations (a) have confirmed that *the center-of-mass diffusivity in an H-polymer follows faithfully that of branch points*, thus validating from first-principles the assumption of the pom-pom model that all friction in an H-molecule is concentrated at the branch points, and (b) predict a dependence of the chain self-diffusion coefficient D_G for entangled H-shaped melts on total chain length N of the form $D_G \propto N^{-b}$, with $b = 2.22$ (± 0.10).

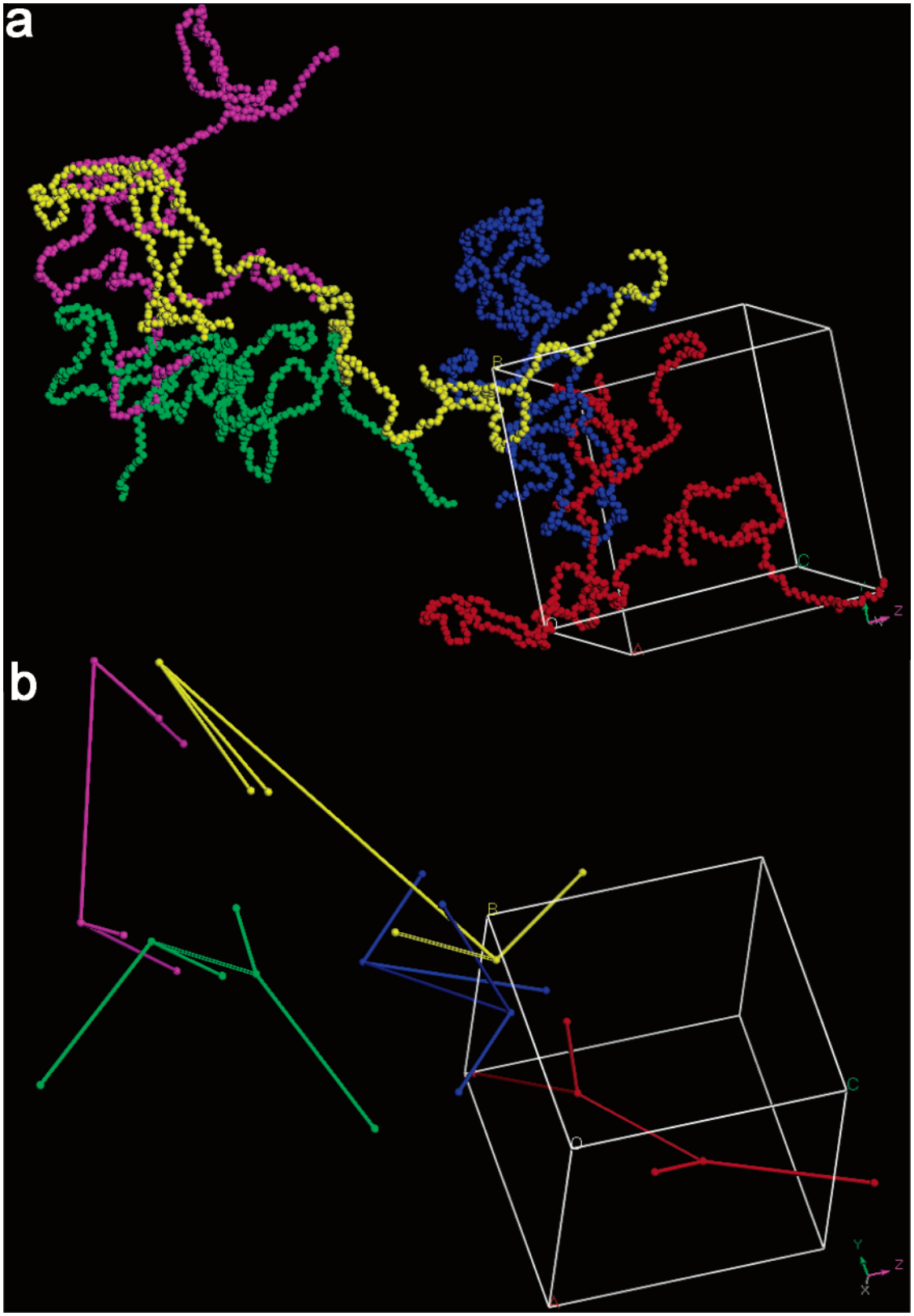

Figure 11. (a) Same as Figure 9a but with chain configurations recorded every 1 μs. (b) Same as Figure 9b but with chain configurations recorded every 1 μs.

Additional results about the msd of the inner backbone segments have shown that entangled H-shaped melts exhibit the four characteristic behaviors proposed by the reptation model for entangled linear polymers. Analyzing the simulation results on the basis of the reptation theory has allowed us to extract the value of the effective tube diameter of the simulated H-shaped PE melts and their reptation time. The results in all cases were compared against available data obtained from similar MD simulation efforts with model linear PE melts of chain length up to C_{500}.

The present study has addressed aspects of equilibrium dynamics of H-shaped polymers bearing unentangled arms. Future work will focus on the simulation

of H-polymers bearing longer, entangled branches, and of q-shaped (i.e., of the type A_3AA_3) molecules in order to study the effect of the number of arms ($q = 2$ vs $q = 3$) on the relaxational properties of the molecule. Efforts are also in progress aiming at simulating the response of these nonlinear systems to an imposed flow field by means of GENERIC MC[58] to probe aspects of the pom-pom model related to arm retraction and branch-point withdrawal.

Acknowledgment. We are indebted to Dow Benelux B.V. for the financial support of this work and the generous allocation of supercomputing time. Fruitful discussions with Dr. Joey Storer (Dow Benelux), Dr. Jaap den Doelder (Dow Benelux), Dr. Martin Kröger (ETH, Zurich), Prof. Doros N. Theodorou (NTUA, Athens), and Prof. Hans Christian Öttinger (ETH, Zurich) are deeply appreciated. The home organizations (ICE/HT-FORTH and University of Patras) are thanked for the allocation of additional CPU time on their multiprocessor workstations. The authors are truly indebted to the Reviewer who suggested analyzing the simulation data for the arm and backbone time autocorrelation functions (ACF's) in the form of ln(−ln(ACF))-vs−ln(t) plots to find the relaxation process(es) associated with arm and backbone orientational relaxation.

References and Notes

(1) Bishko, G.; McLeish, T. C. B.; Harlen, O. G.; Larson, R. G. *Phys. Rev. Lett.* **1997**, *79*, 2352.
(2) McLeish, T. C. B.; Larson, R. G. *J. Rheol.* **1998**, *42*, 81.
(3) McLeish, T. C. B.; Allgaier, J.; Bick, D. K.; Bishko, G.; Biswas, P.; Blackwell, R.; Blottiere, B.; Clarke, N.; Gibbs, B.; Groves, D. J.; Hakiki, A.; Heenan, R. K.; Johnson, J. M.; Kant, R.; Read, D. J.; Young, R. N. *Macromolecules* **1999**, *32*, 6734.
(4) Lohse, D. J.; Milner, S. T.; Fetters, L. J.; Xenidou, M.; Hadjichristidis, N.; Mendelson, R. A.; Garcia-Franco, C. A.; Lyon, M. K. *Macromolecules* **2002**, *35*, 3066.
(5) Bourrigaud, S.; Marin, G.; Poitou, A. *Macromolecules* **2003**, *36*, 1388.
(6) Gabriela, C.; Münstedt, H. *J. Rheol.* **2003**, *47*, 619.
(7) McLeish, T. C. B. *Macromolecules* **1988**, *21*, 1062.
(8) de Gennes, P. G. *J. Chem. Phys.* **1971**, *55*, 572.
(9) Doi, M.; Edwards, S. F. *The Theory of Polymer Dynamics*; Clarendon Press: Oxford, England, 1986.
(10) Roovers, J. *Macromolecules* **1984**, *17*, 1196.
(11) Shie, S. C.; Wu, C. T.; Hua C. C. *Macromolecules* **2003**, *36*, 2141.
(12) Juliani; Archer, L. A. *Macromolecules* **2002**, *35*, 6953; **2002**, *35*, 10048. Archer, L. A.; Juliani. *Macromolecules* **2004**, *37*, 1076.
(13) Doerpinghaus, P. J.; Baird, D. G. *Macromolecules* **2002**, *35*, 10087.
(14) Kapnistos, M.; Vlassopoulos, D.; Roovers, J.; Leal, L. G. *Macromolecules* **2005**, in press.
(15) Karayiannis, N. C.; Mavrantzas, V. G.; Theodorou, D. N. *Phys. Rev. Lett.* **2002**, *88*, 105503.
(16) Karayiannis, N. C.; Giannousaki, A. E.; Mavrantzas, V. G.; Theodorou, D. N. *J. Chem. Phys.* **2002**, *117*, 5465.
(17) Karayiannis, N. C.; Giannousaki, A. E.; Mavrantzas, V. G. *J. Chem. Phys.* **2003**, *118*, 2451.
(18) Mondello, M.; Grest, G. S. *J. Chem. Phys.* **1995**, *103*, 7156.
(19) Mondello, M.; Grest, G. S.; Garcia, A. R.; Silbernagel, B. G. *J. Chem. Phys.* **1996**, *105*, 5208.
(20) Khare, R.; de Pablo, J.; Yethiraj, A. *J. Chem. Phys.* **1997**, *107*, 6956.
(21) Kostov, K. S.; Freed, K. F.; Webb, E. B.; Mondello, M.; Grest, G. S. *J. Chem. Phys.* **1998**, *108*, 9155.
(22) Kioupis, L. I.; Maginn, E. J. *Chem. Eng. J.* **1999**, *74*, 129.
(23) Kioupis, L. I.; Maginn, E. J. *J. Phys. Chem. B* **1999**, *103*, 10781.
(24) MacDowell, L. G.; Vega, C.; Sanz, E. *J. Chem. Phys.* **2001**, *115*, 6220.
(25) Abu-Sharkh, B.; Hussein, I. A. *Polymer* **2002**, *43*, 6333.
(26) Zhang, X. B.; Li, Z. I.; Lu, Z. Y.; Sun, C. C. *Polymer* **2002**, *43*, 3223.
(27) Jabbarzadeh, A.; Atkinson, J. D.; Tanner, R. I. *Macromolecules* **2003**, *36*, 5020.
(28) Zacharopoulos, N.; Economou, I. G. *Macromolecules* **2002**, *35*, 1814.
(29) Bosko, J. T.; Todd, B. D.; Sadus, R. J. *J. Chem. Phys.* **2004**, *121*, 1091.
(30) Bosko, J. T.; Todd, B. D.; Sadus, R. J.*J. Chem. Phys.* **2004**, *121*, 12050.
(31) Peristeras, L. D.; Economou, I G.; Theodorou, D. N. *Macromolecules* **2005**, *38*, 386.
(32) Mavrantzas, V. G. Monte Carlo Simulation of Chain Molecules. In *Handbook of Materials Modeling. Volume 1: Methods and Models*; Yip, S., Ed.; Springer: The Netherlands, 2005; pp 1−15.
(33) Plimpton, S. J. *J. Comput. Phys.* **1995**, *117*, 1.
(34) Large-scale Atomic/Molecular Massively Parallel Simulator (LAMMPS) software distributed by Dr. S. Plimpton at Sandia National Laboratories, US. All MD simulations in this work were carried out using version LAMMPS 2001 (Fortran 90).
(35) Tuckerman, M.; Berne, B. J.; Martyna, G. J. *J. Chem. Phys.* **1992**, *97*, 1990.
(36) Martyna, G. J.; Tuckerman, M.; Tobias, D. J.; Kein, M. L. *Mol. Phys.* **1996**, *87*, 1117.
(37) Martin, M. G.; Siepmann, J. I. *J. Chem. Phys. B* **1998**, *102*, 2569.
(38) Nath, S. K.; Khare, R. *J. Chem. Phys.* **2001**, *115*, 10837.
(39) Nath, S. K.; Escobedo, F. A.; de Pablo, J. J. *J. Chem. Phys.* **1998**, *108*, 9905.
(40) Van der Ploeg, P.; Berendsen, H. J. C. *J. Chem. Phys.* **1982**, *76*, 3271.
(41) Toxvaerd, S. *J. Chem. Phys.* **1997**, *107*, 5197.
(42) Pant, P. V. K.; Theodorou, D. N. *Macromolecules* **1995**, *28*, 7224.
(43) Mavrantzas, V. G.; Boone, T. D.; Zervopoulou, E.; Theodorou, D. N. *Macromolecules* **1999**, *32*, 5072.
(44) Theodorou, D. N. Variable-connectivity Monte Carlo algorithms for the atomistic simulation of long-chain polymer systems. In *Bridging Time Sclaes: Molecular Simulations for the Next Decade*; Nielaba, P., Mareschal, M., Ciccotti, G., Eds.; Springer-Verlag: Berlin, 2002.
(45) Pearson, D. S.; Strate, G. V.; von Meerwall, E.; Schilling, F. C. *Macromolecules* **1987**, *20*, 1133.
(46) Harmandaris, V. A.; Mavrantzas, V. G.; Theodorou, D. N.; Kroger, M.; Ramirez, J.; Öttinger, H. C.; Vlassopoulos, D. *Macromolecules* **2003**, *36*, 1376.
(47) Tsolou, G.; Mavrantzas, V. G.; Theodorou, D. N. *Macromolecules* **2005**, *38*, 1478.
(48) Rouse, P. E. *J. Chem. Phys.* **1953**, *21*, 1272.
(49) Tao, H.; Lodge, T. P.; von Meerwall, E. D. *Macromolecules* **2000**, *33*, 1747.
(50) Pearson, D. S.; Fetters, L. J.; Graessley, W. W.; Strate, G. V.; von Meerwall, E. *Macromolecules* **1994**, *27*, 711.
(51) Lodge, T. P. *Phys. Rev. Lett.* **1999**, *83*, 3218.
(52) Wang, S.-Q. *J. Polym. Sci., Polym. Phys.* **2003**, *41*, 1589.
(53) Likhtman, A. E.; McLeish, T. C. B. *Macromolecules* **2002**, *35*, 6332.
(54) Pütz, M.; Kremer, K.; Grest, G. S. *Europhys. Lett.* **2000**, *49*, 735. Wischnewski, A.; Richter, D. *Europhys. Lett.* **2000**, *52*, 719.
(55) Wischnewski, A.; Monkenbusch, M.; Willner, L.; Richter, D.; Likhtman, A. E.; McLeish, T. C. B.; Farago, B. *Phys. Rev. Lett.* **2002**, *88*, 58301.
(56) Wishnewski, A.; Monkenbusch, M.; Willner, L.; Richter, D.; Kali, G. *Phys. Rev. Lett.* **2003**, *90*, 58302.
(57) Graessley, W. W. *J. Polym. Sci.* **1980**, *18*, 27.
(58) Mavrantzas, V. G.; Öttinger, H. C. *Macromolecules* **2002**, *35*, 960.

MA050989F